

# Quark-hadron phase structure and QCD equations of state in vanishing and finite magnetic field

Abdel Nasser Tawfik\* and Abdel Magied Diab

*Egyptian Center for Theoretical Physics (ECTP),  
Modern University for Technology and Information (MTI), 11571 Cairo, Egypt and  
World Laboratory for Cosmology And Particle Physics (WLCAPP), Cairo, Egypt*

M. T. Hussein

*Physics Department, Faculty of Science, Cairo University, 12613 Giza, Egypt*

In characterizing the quark-hadron phase structure, determining various thermodynamic quantities and investigating their temperature dependencies on vanishing and finite magnetic field, SU(3) Polyakov linear-sigma model (PLSM) is utilized. The dependence of the chiral order-parameter on vanishing and finite magnetic field is calculated in mean-field approximation. In a wide range of temperatures and magnetic field strengths, the thermodynamic observables including trace anomaly, speed of sound squared, entropy density, specific heat and magnetization are presented. An excellent agreement is found when these are confronted to recent lattice QCD calculations. The temperature dependence of these quantities confirms our previous result that the transition temperature is reduced with magnetic field. Furthermore, the temperature dependence of magnetization verifies the conclusion that the QCD matter has paramagnetic properties near and far above the critical temperature. The excellent agreement with recent lattice calculations means that PLSM possesses the correct degrees of freedom in both hadronic and partonic phases and describes well dynamics deriving confined hadrons to deconfined quark-gluon plasma. The magnetic field seems to enhance the occurrence of chiral phase-transition due to its contributions to the Landau quantizations and contribute to the suppression in the chiral condensates relevant to the restoration of the chiral symmetry-breaking. The inverse magnetic catalysis leads to a decrease in the chiral critical temperature with increasing magnetic field. We remark that PLSM has a temperature-limited applicability depending on the temperature-applicability of its chiral and deconfinement order-parameters. Only within this limit the conclusions about equation of state, chiral phase-structure and magnetic properties, etc. can be relatively certain.

PACS numbers: 21.65.Mn, 12.39.Fe, 25.75.Nq, 12.38.Mh, 74.25.N

Keywords: Equations of state in nuclear matter, Chiral Lagrangian, Quark confinement, Quark-gluon plasma, Response to electromagnetic fields

## Contents

<b>I. Introduction</b>	2
<b>II. SU(3) Polyakov Linear-sigma Model</b>	3
<b>III. Results and discussion</b>	6
A. PLSM and lattice QCD order parameters in vanishing and finite magnetic field	6
1. Chiral and deconfinement order-parameters	6
2. Subtracted condensates	7
B. Thermodynamic properties in vanishing and finite magnetic field	8
1. Trace anomaly	10
2. Speed of sound squared	11
3. Entropy	12
4. Specific heat	12

---

\*Electronic address: a.tawfik@eng.mti.edu.eg

5. Magnetization and magnetic catalysis	14
<b>IV. Conclusions</b>	15
<b>References</b>	16

## I. INTRODUCTION

The structure of quantum chromodynamic (QCD) matter at very high temperatures [much higher than the critical temperature ( $T_c$ ), which characterizes the hadron-quark deconfinement phase-transition] is well understood by perturbation theory, for instance. But the entire quark-hadron phase structure still represents a great challenge to lattice QCD and particle scientists. On one hand, it is difficult to draw predictions for the properties of QCD matter, especially the partonic matter, at arbitrary finite temperatures and chemical potentials. The reason is that QCD under extreme conditions of temperatures and densities remains strongly coupled. On the other hand, non-perturbative approaches, such as lattice QCD simulations, the only available first-principles calculation-tools, turn to be very reliable, especially at vanishing chemical potential. This predicts that the crossover to the quark-gluon plasma (QGP) occurs at  $T \sim \mathcal{O}(m_\pi)$  and might be tolerated to be implemented at finite chemical potentials but much less than the temperatures. However, this approach can't be used at higher chemical potentials and lower temperatures which characterize the color-superconducting phase structure, for instance.

Alternatively, the models that incorporate some of QCD properties are easier to be implemented in order to draw even a rough picture about the quark-hadron phase structure that might occur at almost arbitrary finite temperature and chemical potential. Nambu-Jona-Lasinio models [1, 2], which exclude the gluonic degrees of freedom and replace the strong interaction by four-fermion interaction, are widely-used effective models. Another approach is the (non)linear-sigma model, which was introduced by Gell-Mann and Levy [3] as a Lagrangian theory of maps. In this QCD-like model, the spinless sigma meson, the scalar which was introduced earlier by Schwinger, largely gives the degrees of freedom and is allowed to be mapped to a (non)linear manifold called the target manifold. This model is a prototype of spontaneous symmetry breaking and describes the quarks interaction through the exchange of pion- and sigma-meson fields. The present paper is devoted to the utilization of mean field approximation of SU(3) Polyakov linear-sigma model (PLSM) in order to characterize the quark-hadron phase structure by calculating the chiral order-parameter ( $M_b$ ), and the light and strange quarks net-condensate ( $\Delta_{l,s}$ ) at finite temperature and vanishing chemical potential.

Due to oppositely flying of charges approaching relativistic energy limits especially in off-central collisions of heavy ions, a huge magnetic field can be created in heavy-ion collision (HIC) experiments. Because of the very short spending (life-time) of the evolution of such magnetic field, it is assumed to have almost no effect on the detector and its external magnet but remarkable influences on the strongly interacting QCD matter. In addition to hot and dense QCD matter, the influence of a strong magnetic field ( $eB$ ) on the structure of QCD matter is also a very interesting subject. This kind of investigation has realistic relevance to phenomenology of relativistic heavy-ion collisions in which a strong magnetic field is produced in non-central collisions [4, 5]. Moreover, the expected values of the magnetic field strengths in the different HIC experiments such as superproton synchrotron (SPS), relativistic heavy-ion collider (RHIC) and large hadron collider (LHC) ranges between  $0.1 m_\pi^2$  to  $m_\pi^2$  and  $10 - 15 m_\pi^2$ , respectively [5, 6], where  $m_\pi^2 \simeq 10^{19}$  Gauss.

Concerning the phenomenologically interesting consequence from the magnetic field effect on the QCD matter, there have been many investigations. The Large Hadron Collider (LHC), at CERN, provides a possible signature of the CP violation and chiral symmetry restoration [7, 8]. The QCD vacuum properties have been also studied by means of the holographic QCD models [9], Chiral Magnetic Effect (CME) [4, 10]. The presence of a magnetic field have been investigated previously within different frameworks, mainly using effective models [11–16], especially the NJL model [16–21], PLSM [22–24] and chiral perturbation theory ( $\chi$ PT) [21, 25, 26].

Recently, various QCD-like models have been devoted to study the influences of finite magnetic field on the strongly interacting QCD matter at finite temperature [21–24, 30, 32–34]. These can be compared with the studies on vanishing magnetic field [27–29, 31]. Many of these studies have investigated the quark-hadron phase-transition in thermal and dense medium, which are conjectured to improve the description of the QCD phase-diagram. Following this procedure, we perform our calculations for the quark-hadron phase-structure and QCD equation of state (EoS) from PLSM. Furthermore, we compare our results with the available recent lattice QCD calculations in zero [35] and in nonzero magnetic field [36].

The SU(3) PLSM is utilized to characterize the respective influences of the magnetic field on the quark-hadron phase-transition in a wide range of temperatures. Prior to confronting our results to lattice QCD, we show that the order parameters have a reasonable agreement with the lattice simulations. We also confront the various thermodynamic quantities to different lattice QCD calculations. The characterization of the hadronic equation of state has been discussed in Ref. [37, 38]. It was concluded that the characteristics of the speed of sound squared  $c_s^2 = \partial p / \partial \epsilon = s / c_v$  and  $p / \epsilon$  ratio. Both are distinguishable below and above  $T_c$ . Below  $T_c$ , the thermal behavior of the speed of sound squared matches the  $p / \epsilon$  ratio. Above  $T_c$ , the value of  $c_s^2 = s / c_v$  becomes larger than that of  $p / \epsilon$ . At very high temperatures, both quantities get very close to each other and likely approach the asymptotic value, i.e.,  $1/3$  [39].

Applying finite magnetic field on QCD matter allows the description of important phenomenon such as the chiral magnetic effect (CME) and the magnetic catalysis [40–44]. CME is strongly related to the electric charge separation phenomenon that probably become measurable in HIC experiments such as PHENIX [45] and STAR [46–49] at RHIC and ALICE at LHC [50]. The magnetic catalysis characterizes the dependence of  $T_c$  on the magnetic field strength.

The present paper is organised as follows. In section II, SU(3) PLSM in thermal and dense medium with and without magnetic field shall be introduced. The comparison of PLSM order parameters with the lattice QCD calculations shall be discussed in section III A. The results of various thermodynamic quantities in zero and nonzero magnetic field shall be elaborated in section III B. Section IV is devoted to the final conclusions.

## II. SU(3) POLYAKOV LINEAR-SIGMA MODEL

The linear-sigma model is a widely acceptable approach for the investigation of meson states [28]. The chiral SU(3) LSM Lagrangian with  $N_f = 2 + 1$  consists of two parts;  $\mathcal{L}_{chiral} = \mathcal{L}_q + \mathcal{L}_m$ .

- The first term expresses the quark contributions, Eq. (1), which are coupled with a flavor-blind Yukawa coupling  $g$  [51], i.e., quarks couple to mesons,

$$\mathcal{L}_q = \sum_f \bar{q}_f (i\gamma^\mu D_\mu - gT_a(\sigma_a + i\gamma_5\pi_a))q, \quad (1)$$

- while the second term gives the meson contributions

$$\mathcal{L}_m = \text{Tr}(\partial_\mu \Phi^\dagger \partial^\mu \Phi - m^2 \Phi^\dagger \Phi) - \lambda_1 [\text{Tr}(\Phi^\dagger \Phi)]^2 - \lambda_2 \text{Tr}(\Phi^\dagger \Phi)^2 + c[\text{Det}(\Phi) + \text{Det}(\Phi^\dagger)] + \text{Tr}[H(\Phi + \Phi^\dagger)], \quad (2)$$

where  $\Phi$  is  $3 \times 3$  matrix includes the nonet meson states as

$$\Phi = \sum_{a=0}^{N_f^2-1} T_a(\sigma_a - i\pi_a). \quad (3)$$

The number of generators ( $T_a$ ) is defined according to the number of quark flavors ( $N_f$ ). At  $N_f = 3$ , the chiral Lagrangian contains unitary matrices with  $SU(3)_r \times SU(3)_l$  symmetry [52]. In U(3) algebra,  $T_a$  is determined by Gell-Mann matrices  $\hat{\lambda}_a$  [52];  $T_a = \hat{\lambda}_a / 2$  with  $a = 0, \dots, 8$ .

LSM can be coupled to Polyakov-loop potential in order to incorporate deconfinement phase-transition in the QCD system by adding color-gluon interaction such that  $\mathcal{L} = \mathcal{L}_{chiral} - \mathcal{U}$ . Thus, the added Polyakov-loop potential should be fine-tuned through confrontation with lattice QCD simulations. Furthermore, it should have  $Z(3)$  symmetry [10, 54–56]. For example in pure gauge limit, a temperature-dependent potential can be used;  $U(\phi, \phi^*, T)$ . Its  $Z(3)$  center symmetry should be similar to that of the pure gauge QCD Lagrangian [55, 60]. The trace of color space of Polyakov loop determines the creation operator of a static quark at the spatial position  $\vec{x}$ . The color charges and gluons dynamics can then be given in dependence on the thermal expectation value of a color-traced Wilson-loop in the temporal direction [57],

$$\phi = \langle \text{Tr}_c \mathcal{P}(\vec{x}) \rangle / N_c, \quad \phi^* = \langle \text{Tr}_c \mathcal{P}^\dagger(\vec{x}) \rangle / N_c. \quad (4)$$

Then, the Polyakov loop operator becomes identical to the Wegner-Wilson loop [57],

$$\mathcal{P}(\vec{x}) = \mathcal{P} \exp \left[ i \int_0^{1/T} d\tau A_0(\vec{x}, \tau) \right], \quad (5)$$

where  $A_0(\vec{x}, \tau)$  is the temporal component of the Euclidean gauge field  $A_\mu$  [57, 58] and  $\tau$  denotes the Euclidean time component. It was found that enlarging  $N_c$  decreases the critical temperature of the deconfinement phase-transition [28]. Thus, the Polyakov loops  $\phi$  and  $\phi^*$  can be considered as order parameters for the deconfinement phase-transition [55, 60].

There are different potential types for the Polyakov loop [10, 55, 56, 60]. In the present work, we implement the polynomial form,

$$\frac{\mathcal{U}_{\text{poly}}(\phi, \phi^*, T)}{T^4} = -\frac{b_2(T)}{2} \left( |\phi|^2 + |\phi^*|^2 \right) - \frac{b_3}{6} (\phi^3 + \phi^{*3}) + \frac{b_4}{16} \left( |\phi|^2 + |\phi^*|^2 \right)^2, \quad (6)$$

where  $b_2(T) = a_0 + a_1 (T_0/T) + a_2 (T_0/T)^2 + a_3 (T_0/T)^3$ . With the parameters  $a_0 = 6.75$ ,  $a_1 = -1.95$ ,  $a_2 = 2.625$ ,  $a_3 = -7.44$ ,  $b_3 = 0.75$  and  $b_4 = 7.5$  [55], the pure gauge QCD thermodynamics is well reproduced. For a better agreement with lattice QCD simulations, the critical temperature  $T_0$  is fixed at 187 MeV for  $N_f = 2+1$  [60]. The possible differences in the critical temperatures;  $T_0 = 187$  MeV in the PNJL model and 220 MeV in the PLSM can be understood due to the introduction of quarks which leads to decreasing the deconfinement temperature in the pure gauge limit. In both models the Polyakov potential  $U$  should be the same.

$m_\sigma$ [MeV]	$c$ [MeV]	$h_l$ [MeV <sup>3</sup> ]	$h_s$ [MeV <sup>3</sup> ]	$m^2$ [MeV <sup>2</sup> ]	$\lambda_1$	$\lambda_2$
800	4807.84	(120.73) <sup>3</sup>	(336.41) <sup>3</sup>	-(306.26) <sup>2</sup>	13.49	46.48

**Tab. I:** Summary of PLSM's parameters. A detailed description is given in Ref. [64]

In thermal equilibrium, the exchanges of energy between particles and antiparticles can be described by path integral over quark, antiquark and meson fields. Thus, the grand canonical partition function reads

$$\mathcal{Z} = \int \prod_a \mathcal{D}\sigma_a \mathcal{D}\pi_a \int \mathcal{D}\psi \mathcal{D}\bar{\psi} \exp \left[ \int_x (\mathcal{L} + \sum_{f=u,d,s} \mu_f \bar{\psi}_f \gamma^0 \psi_f) \right], \quad (7)$$

where  $\int_x \equiv i \int_0^{1/T} dt \int_V d^3x$  with  $V$  being the volume of the system and  $\mu_f$  is the chemical potential for quark flavors  $f = (u, d, s)$ . In addition, we assume symmetric quark matter and degenerate light quarks, therefore we can define a uniform blind chemical potential  $\mu_f \equiv \mu_{u,d} = \mu_s$  [51, 53, 64].

The purely mesonic potential is given as a function to non-strange ( $\sigma_l$ ) and strange ( $\sigma_s$ ) quark-flavor basis

$$U(\sigma_l, \sigma_s) = -h_l \sigma_l - h_s \sigma_s + \frac{m^2 (\sigma_l^2 + \sigma_s^2)}{2} - \frac{c \sigma_l^2 \sigma_s}{2\sqrt{2}} + \frac{\lambda_1 \sigma_l^2 \sigma_s^2}{2} + \frac{(2\lambda_1 + \lambda_2) \sigma_l^4}{8} + \frac{(\lambda_1 + \lambda_2) \sigma_s^4}{4}. \quad (8)$$

The quark and antiquark contribution can be divided into two regimes:

- At zero magnetic field ( $eB = 0$ ) with finite temperature ( $T$ ) and chemical potential ( $\mu_f$ ) [61]

$$\Omega_{\bar{q}q}(T, \mu_f) = -2T \sum_{f=l,s} \int_0^\infty \frac{d^3\vec{P}}{(2\pi)^3} \left\{ \ln \left[ 1 + 3 \left( \phi + \phi^* e^{-\frac{E_f - \mu_f}{T}} \right) \times e^{-\frac{E_f - \mu_f}{T}} + e^{-3\frac{E_f - \mu_f}{T}} \right] \right. \\ \left. + \ln \left[ 1 + 3 \left( \phi^* + \phi e^{-\frac{E_f + \mu_f}{T}} \right) \times e^{-\frac{E_f + \mu_f}{T}} + e^{-3\frac{E_f + \mu_f}{T}} \right] \right\}, \quad (9)$$

where  $E = \sqrt{\vec{P}^2 + m_f^2}$  is the dispersion relation of the valence quark and antiquark and  $m_f$  is the  $f$ -th mass of quark flavor, which is respectively related to light and strange chiral condensates

$$m_l = g \sigma_l / 2 \qquad m_s = g \sigma_s / \sqrt{2}, \quad (10)$$

where subscript  $l$  refers to degenerate light quarks and  $s$  to strange quark.

- At nonzero magnetic field ( $eB \neq 0$ ) with finite  $T$  and  $\mu_f$ , the concepts of Landau quantization and magnetic catalysis, where the magnetic field is assumed to be oriented along  $z$ -direction, should be implemented.

In doing this, Landau-level structure of energy levels in finite magnetic field is conjectured to affect the phase space [40],

$$\int \frac{d^3p}{(2\pi)^3} \longrightarrow \frac{|q_f|B}{2\pi} \sum_{\nu} \int \frac{dP_z}{2\pi} (2 - \delta_{0\nu}), \quad (11)$$

where  $\nu$  stands of Landau quantization levels and  $q_f$  is the corresponding electric charge of  $f$ -th quark flavors. At  $eB \neq 0$ , the quarks and antiquark potential becomes

$$\begin{aligned} \Omega_{\bar{q}q}(T, \mu_f, B) = & -2 \sum_{f=l,s} \frac{|q_f|BT}{(2\pi)^2} \sum_{\nu=0}^{(\nu_{max})_f} (2 - \delta_{0\nu}) \int_0^{\infty} dP_z \\ & \left\{ \ln \left[ 1 + 3 \left( \phi + \phi^* e^{-\frac{E_{B,f}-\mu_f}{T}} \right) e^{-\frac{E_{B,f}-\mu_f}{T}} + e^{-3\frac{E_{B,f}-\mu_f}{T}} \right] \right. \\ & \left. + \ln \left[ 1 + 3 \left( \phi^* + \phi e^{-\frac{E_{B,f}+\mu_f}{T}} \right) e^{-\frac{E_{B,f}+\mu_f}{T}} + e^{-3\frac{E_{B,f}+\mu_f}{T}} \right] \right\}, \quad (12) \end{aligned}$$

where  $E_{B,f}$  is the dispersion relation of  $f$ -th quark-flavor in nonzero magnetic field

$$E_{B,f} = [P_z^2 + m_f^2 + |q_f|(2n + 1 - \sigma)B]^{1/2}, \quad (13)$$

with  $n$  is the quantization number known as the Landau quantum number and  $\sigma$  is related to the spin quantum-number,  $\sigma = \pm S/2$ . It is noteworthy highlighting that, the quantity  $2n + 1 - \sigma$  can be replaced by a summation over the Landau Levels  $0 \leq \nu \leq \nu_{max_f}$ . The earlier is the Lowest Landau Level, while the latter stands for the Maximum Landau Level ( $(\nu_{max})_f$ ). For the sake of completeness, we mention that  $2 - \delta_{0\nu}$  represents degenerate Landau Levels.  $\nu_{max_f}$  contributes to the maximum quantization number ( $\nu_{max_f} \rightarrow \infty$ ). Quark charges, magnetic fields, temperatures, and baryon chemical potentials influence the maximum occupation of the Landau levels [62]. In Ref. [24], we have discussed on how the Landau levels are filled up in finite magnetic field. Also, we have concluded that increasing Landau levels very slightly sharpens the phase transition and decreases the critical temperature [24].

The inclusion of the fermion vacuum term causes second-order phase-transition in the chiral limit and other significant effects on the phase structure, which is commonly referred to as no-sea approximation [63] and conjectured to distort the critical behavior, especially at the chiral phase-transition. When the fermion vacuum term is included, the transition can be of first- or second-order depending on the choice of coupling constants and on the baryon density. In Ref. [63], the authors discussed on the thermodynamical differences between NJL and quark-meson (QM) models or LSM. In this approximation, the adiabatic trajectories obtained from the QM model exhibit a *kink* at the chiral crossover phase-transition, while from the NJL model, it is *smooth* everywhere [51]. This effect underlies a first-order phase-transition from the LSM model in the chiral limit, especially when the fermionic vacuum fluctuations are neglected [85].

Equations (9) and (12) in vanishing and finite magnetic field, respectively, give the fermionic contributions to the medium. The formal way of removing the ultraviolet divergences is covered through the fermion vacuum term [20] in sharp noncovariant cut-off  $\Lambda$  [20],

$$\Omega_{\bar{q}q}^{\text{vac}} = 2N_c N_f \sum_f \int_{\Lambda} \frac{d^3p}{(2\pi)^3} E_f = \frac{-N_c N_f}{8\pi^2} \sum_f \left( m_f^4 \ln \left[ \frac{\Lambda + \epsilon_{\Lambda}}{m_f} \right] - \epsilon_{\Lambda} [\Lambda^2 + \epsilon_{\Lambda}^2] \right), \quad (14)$$

where  $\epsilon_{\Lambda} = (\Lambda^2 + m_f^2)^{1/2}$  and  $m_f$  is the flavor mass, with subscript  $f$  running over light ( $l$ ) and strange ( $s$ ) quark flavors, Eq. (10). In finite magnetic field, we find that the fermion vacuum term has a negligible effect on the PLSM results.

PLSM has seven parameters  $m^2$ ,  $h_l$ ,  $h_s$ ,  $\lambda_1$ ,  $\lambda_2$ , and  $c$ , a coupling  $g$ , two condensates  $\sigma_l$  and  $\sigma_s$  and two order parameters  $\phi$  and  $\phi^*$  to be determined. The first six parameters can be fixed from experiments. Tab. I summarizes the values of these six parameters at sigma mass  $m_{\sigma} = 800$  MeV [64].

Furthermore, the free energy at finite volume ( $V$ ) and finite magnetic field ( $eB$ ) is defined as  $\mathcal{F} = -T \cdot \log[\mathcal{Z}]/V$ . From Eqs. (6), (8), (9) and (12) [22]

$$\mathcal{F} = U(\sigma_l, \sigma_s) + \mathcal{U}(\phi, \phi^*, T) + \Omega_{\bar{q}q}(T, \mu_f, B) + \delta_{0,eB} \Omega_{\bar{q}q}(T, \mu_f). \quad (15)$$

In order to determine  $\sigma_l$ ,  $\sigma_s$ ,  $\phi$  and  $\phi^*$ , the free energy  $\mathcal{F}$ , Eq. (15), should be minimized with respect to  $\sigma_l$ ,  $\sigma_s$ ,  $\phi$  and  $\phi^*$ , respectively

$$\left. \frac{\partial \mathcal{F}}{\partial \sigma_l} = \frac{\partial \mathcal{F}}{\partial \sigma_s} = \frac{\partial \mathcal{F}}{\partial \phi} = \frac{\partial \mathcal{F}}{\partial \phi^*} \right|_{min} = 0, \quad (16)$$

meaning that  $\sigma_l = \bar{\sigma}_l$ ,  $\sigma_s = \bar{\sigma}_s$ ,  $\phi = \bar{\phi}$  and  $\phi^* = \bar{\phi}^*$  are global minimum.

### III. RESULTS AND DISCUSSION

#### A. PLSM and lattice QCD order parameters in vanishing and finite magnetic field

##### 1. Chiral and deconfinement order-parameters

The chiral condensate  $\sigma_l$  and  $\sigma_s$  and deconfinement order-parameters  $\phi$  and  $\phi^*$  can be estimated from global minimization of thermodynamic potential, Eq. (16). For more details about the calculations of  $\sigma_l$ ,  $\sigma_s$ ,  $\phi$  and  $\phi^*$  from PLSM, the readers are kindly advised to consult Refs. [23, 27–29]. In doing this, we use  $\sigma_{l_0} = 92.4$  MeV and  $\sigma_{s_0} = 94.5$  MeV.

Furthermore, PLSM can be utilized in determining the physical masses of degenerate light and strange quarks under the assumption that the quark chemical potentials are equivalent to each other,  $\mu_u = \mu_d = \mu_s$ . It is worthwhile to devote further efforts in order to determine the correlations and the fluctuations between the chiral and deconfinement phase-transition(s).

Fig. 1 depicts the normalized chiral condensates,  $\sigma_l/\sigma_{l_0}$  and  $\sigma_s/\sigma_{s_0}$ , respectively, in presence of Polyakov-loop potential (characterizing the deconfinement phase-transition). At vanishing chemical potential ( $\mu = 0$  MeV), the two Polyakov-loops are identical;  $\langle \phi \rangle = \langle \phi^* \rangle$ . The order parameters are estimated from PLSM at vanishing chemical potential and finite magnetic field strength for a wide range of temperatures. Fig. 1 shows the temperature dependence of the chiral condensate and that of deconfinement phase-transitions in vanishing [right-hand panel (a)]  $eB = 0.0$ , and finite magnetic fields  $eB = 0.1$  [middle panel (b)] and finite magnetic field  $eB = 0.3$  GeV<sup>2</sup> [left-hand panel (c)], respectively.

In order to determine the chiral temperature ( $T_\chi$ ), two procedures can be followed:

- looking for the intersection of chiral and deconfinement order-parameters, Fig. 1.
- locating the peak in the temperature dependence of strange and nonstrange chiral condensates (not illustrated in the present work). For details the readers can consult Ref. [23].

The chiral temperature is defined as the temperature, at which restoration of broken chiral-symmetry for light-quark condensate ( $T_\chi^{(l)}$ ) and for strange-quark condensate ( $T_\chi^{(s)}$ ) takes place.

Tab. II summarizes the approximate estimation for the chiral temperatures at different magnetic field strengths but vanishing chemical potential.  $T_\chi^{(l)}$  and  $T_\chi^{(s)}$  are chiral temperatures at which the deconfinement phase-transition and either light ( $l$ ) and strange ( $s$ ) chiral-condensate intersect, see Fig. 1 and left-hand panel of Fig. 7. With increasing the magnetic field strength, we observe that the the chiral temperature of light-quark condensate  $T_\chi^{(l)}$  decreases faster than that of strange-quark condensate. In other words, increasing the magnetic field strength contributes to the suppression in the chiral condensate, i.e., the restoration of broken chiral symmetry takes place at lower temperatures. The earliness of chiral phase-transition relative to lower temperature (or chiral condensate suppression) is known as inverse magnetic catalysis (IMC).

	$eB = 0.0$ GeV <sup>2</sup>	$eB = 0.1$ GeV <sup>2</sup>	$eB = 0.3$ GeV <sup>2</sup>
$T_\chi^{(l)}$ [MeV]	177.8	150.4	122.76
$T_\chi^{(s)}$ [MeV]	218.6	217.6	217.05

**Tab. II:** Approximate estimation for the chiral temperatures at different magnetic fields.

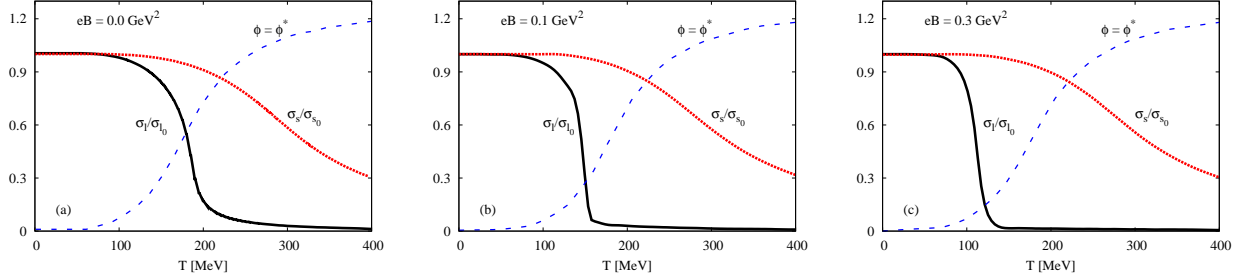


**Fig. 1:** (Color online) The normalized chiral condensates  $\sigma_l/\sigma_{l0}$  and  $\sigma_s/\sigma_{s0}$  (solid and dotted curves, respectively) and the Polyakov-loop potential, the order-parameters  $\phi$  and  $\phi^*$  (dashed curve) are given as functions of temperature at different magnetic fields  $eB = 0.0$  [left-hand panel (a)],  $eB = 0.1$  [middle panel (b)] and  $eB = 0.3 \text{ GeV}^2$  [right-hand panel (c)], respectively.

## 2. Subtracted condensates

The lattice QCD simulations combine both light- and strange-quark condensates [65],

$$\Delta_{l,s} = \frac{\langle \bar{l}l \rangle - \left(\frac{m_l}{m_s}\right) \langle \bar{s}s \rangle \Big|_T}{\langle \bar{l}l \rangle - \left(\frac{m_l}{m_s}\right) \langle \bar{s}s \rangle \Big|_{T=0}}, \quad (17)$$

where  $\langle \bar{q}q \rangle$  and  $m_q$  stand for antiquark-quark condensate and quark mass, respectively, with  $q \in [l, s]$ . This quantity reads the ratio of net light- to strange-quark condensates at finite temperature ( $T$ ) to the net of light- to strange-quark condensates at  $T = 0$  [68]. It is apparent that the dependence of the quark masses ( $m_q$ ) on the corresponding chiral condensates at vanishing and finite temperature is essential.

In the present work, we introduce calculations for degenerate light-quarks and heavy strange-quark from SU(3) PLSM.

$$\Delta_{l,s} = \frac{\sigma_l - \left(\frac{h_l}{h_s}\right) \sigma_s \Big|_T}{\sigma_l - \left(\frac{h_l}{h_s}\right) \sigma_s \Big|_{T=0}}, \quad (18)$$

where the flavor masses  $m_l$  and  $m_s$  are replaced by the explicit breaking strengths  $h_l$  and  $h_s$ , respectively. Furthermore, the lattice QCD simulations define the chiral order-parameter in terms of the chiral condensate [66],

$$M_b = \frac{m_s \langle \bar{\sigma}_l(T, \mu) \rangle}{T^4}. \quad (19)$$

The left-hand panel of Fig. 2 (a) presents the subtracted chiral-condensates as a function of temperature at vanishing chemical potential and magnetic field  $eB = 0.0$  (solid curves) and compares the PLSM results with various (2 + 1) lattice QCD simulations, in which asqtad [69] and p4 [70, 71] improved staggered fermion actions with almost physical strange and light-quark masses and temporal extension  $N_\tau = 8$  are utilized. The agreement between both sets of calculations is excellent. The steeper decline in the subtracted chiral-condensate comes from the pure gauge potential in the grand canonical calculations in absence of the gluons interactions. We observe that  $\Delta_{l,s}$  possesses a constant finite value at low  $T$ . When the temperature approaches about half  $T_c$ ,  $\Delta_{l,s}$  begins to decrease with increasing temperature. This signal indicates the liberation of the quark and gluon degrees of freedom. The hadron deconfinement and the restoration of broken chiral symmetry are conjectured to take place at  $T_c$ .

It is noteworthy emphasizing that the introduction of the Polyakov-loop correction improves the calculation of the pure gauge potential through improving the gluon contributions to the interaction. The latter leads to a smooth chiral-transition or a repaid crossover [69–71].

The right-hand panel of Fig. 2 (b) shows the temperature dependence of  $M_b$ . As introduced,  $M_b$ , Eq. (19), combines the mass of strange quark ( $m_s$ ) with the light-quark condensate ( $\sigma_l$ ) normalized to  $T^4$ . The PLSM calculations are compared with HISQ/tree lattice QCD with  $N_\tau = 8$  and two values for the quark masses,

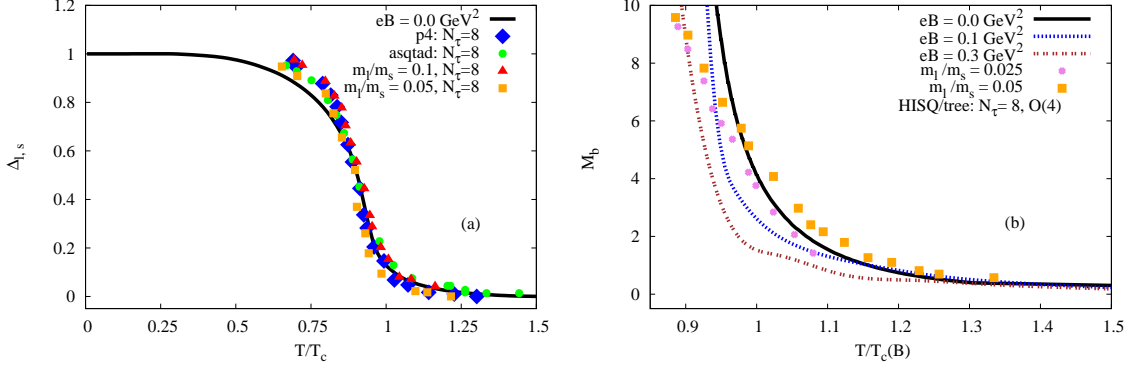


**Fig. 2:** (Color online) Left-hand panel (a): the subtracted condensate (light- and strange-quark net-condensate)  $\Delta_{l,s}$  given as a function of temperature at vanishing chemical potential and vanishing magnetic field  $eB = 0.0 \text{ GeV}^2$  (solid curves) compared with lattice QCD calculations (symbols) [67, 68]. Right-hand panel (b): the chiral order-parameter,  $M_b$ , Eq. (19), at different values of magnetic field  $eB = 0.0$  (solid curves),  $eB = 0.1$  (dotted curves),  $eB = 0.2$  (dashed curves),  $eB = 0.3$  (double-dotted curves) compared with HISQ/tree lattice QCD with  $N_\tau = 8$  and two values for the quark masses,  $M_q/M_s = 0.025$  (close circle) and  $M_q/M_s = 0.05$  (close square) [66].

$M_q/M_s = 0.025$  (close circle) and  $M_q/M_s = 0.05$  (close square) [66]. The agreement between the two sets of calculations is convincing, especially in vanishing magnetic field (solid curve) and in the crossover region, in which the rapid decline in  $M_b$  indicates a smooth phase-transition from finite to vanishing  $M_b$ .

### B. Thermodynamic properties in vanishing and finite magnetic field

The thermodynamic observables can be deduced from the total free energy, Eq. (15). For instance, the pressure at finite  $T$  and  $eB$  but vanishing  $\mu$  defines the free energy of the system of interest

$$p(T, eB) = -\mathcal{F}(T, eB). \quad (20)$$

The free-energy density  $f = \mathcal{F}/V$  at  $eB = 0$  can be given as

$$f = \epsilon - Ts, \quad (21)$$

where  $\epsilon$  and  $s$  being energy density and entropy density, respectively. At finite magnetic field  $\mathbf{B} = B \hat{e}_z$  directed along the  $z$ -axis, the free energy density reads [72]

$$f = \epsilon^{\text{tot}} - \epsilon^{\text{field}} - Ts = \epsilon^{\text{tot}} - Ts - eB \mathcal{M}, \quad (22)$$

where  $\epsilon^{\text{tot}} = \epsilon + \epsilon^{\text{field}}$  is the total energy density consisting of energy density ( $\epsilon$ ) characterizes the system of interest and  $\epsilon^{\text{field}} = eB\mathcal{M}$  stemming from the influence of the magnetic field and  $\mathcal{M}$  is the magnetization. The magnetic field  $eB$  is given in the units of the elementary charge  $|e| > 0$ .

We recall that in vanishing magnetic field, the partition function is given by an integral over the six-dimensional phase-space and integral over the dispersion relations. In this case, the energy-momentum dispersion relation,  $E_f$ , follows the Lorentz invariance principle, but in finite magnetic field, the integral is dimensionality reduced and simultaneously accompanied by a considerable modification in the dispersion relations, themselves. At finite magnetic field  $eB$ , the velocity of a test particle with momentum  $\partial\epsilon^{\text{tot}}/\partial p$  can be deduced from the dispersion relations,

$$v_{P_z} = c \left[ \frac{c P_z}{c P_z + 2|q_f|(\nu + \frac{1}{2} - \frac{\sigma}{2})B} \right]. \quad (23)$$

The Lorentz invariance principle can be tested through the velocity of a test particle with momentum  $p$ . The causality is apparently guaranteed as  $v_{P_z}$  does not exceed the speed of light ( $c$ ), i.e., as long as as the  $eB$ -term

is finite positive, which should be estimated, quantitatively, as a function of temperature and magnetic field strength.

Form Eq. (22), the entropy density and the magnetization can be obtained as

$$s = -\frac{1}{V} \frac{\partial \mathcal{F}}{\partial T}, \quad (24)$$

$$\mathcal{M} = -\frac{1}{V} \frac{\partial \mathcal{F}}{\partial (eB)}. \quad (25)$$

The corresponding differential relation for pressure is to some extent involved. As the magnetic field marks a preferred direction, the pressure  $p_i$  might be different along the geometrical effect of the magnetic field. The magnetic field is directed along the  $z$ -direction. The volume of the system reads as  $V = L_x L_y L_z$ . Thus, lattice QCD simulations distinguish between two different systems:

- B-scheme: the magnetic field is kept fixed in all direction leading to an isotropic pressure

$$p_x = p_y = p_z = -f \quad (26)$$

- $\Phi$ -scheme: the magnetic flux ( $\Phi = eB \cdot L_x L_y$ ) is kept fixed leading to an anisotropic pressure

$$p_x = p_y = p_z - eB \cdot \mathcal{M} \quad (27)$$

Accordingly, the thermodynamic quantities should be corrected. For instance, the trace anomaly (interaction measure) in  $\Phi$ -scheme becomes

$$I = \epsilon - 3p_z + 2eB \cdot \mathcal{M}. \quad (28)$$

The speed of sound squared ( $c_s^2$ ) is an essential thermodynamic quantity to be estimated. It determines the equation of state  $p(\epsilon)$  [38], where at a constant entropy it reads

$$c_s^2 = \left( \frac{\partial p}{\partial \epsilon} \right)_s = \frac{\partial p}{\partial T} / \frac{\partial \epsilon}{\partial T} = \frac{s}{c_v}. \quad (29)$$

The specific heat ( $c_v$ ) gives the thermal rate change of the energy density at a constant volume.

The Stefan-Boltzmann (SB) limits can be deduced from the lowest-order perturbation theory. For massless quarks and gluons [61]

$$T \log \mathcal{Z}(V, T, \mu) = \frac{g_f V}{12} \left( \frac{7}{30} \pi^2 T^4 + T^2 \mu^2 + \frac{1}{2 \pi^2} \mu^4 \right) + g_b V \frac{\pi^2}{90} T^4, \quad (30)$$

where  $g_f$  and  $g_b$  are the degrees of freedom of quarks and gluons, respectively. In finite magnetic field ( $eB$ ) [36]

$$T \log \mathcal{Z}(V, T, \mu, eB) = \frac{19 V \pi^2}{36} T^4 + b_1^{\text{free}} (eB)^2 V \log \left( \frac{T}{\Lambda_H} \right) + \dots, \quad (31)$$

where  $b_1^{\text{free}}$  is a parameter to be fixed by leading-order perturbation theory and  $\Lambda_H = 0.12$  GeV is a renormalization scale [36]. The latter appears in the perturbation terms, exclusively.

The present work illustrates the capability of PLSM in reproducing recent lattice QCD calculations, which can be characterized as follows.

- In finite magnetic field, the equation of state from  $(2+1)$  lattice QCD calculations with physical quark masses has been determined [36], as given in right-hand panel of Figs. 3, 4, 5 and Fig. 7. The equation of state is sensitive to the change in the control parameters of the system. These parameters include temperature, chemical potentials corresponding to the various conserved charges and, as in the present work, the presence of magnetic field along longitudinal direction  $\mathbf{B} = B \hat{e}_z$ . The lattice calculations use tree-level improved Symanzik gauge action, and stout improved staggered quarks in the fermionic sector, fixed ratio of light- and strange-quark masses,  $m_l = m_s/28$  and lattice size  $N_\sigma^3 \times N_\tau$ .

- The lattice QCD results presented in the left-hand panel of Figs. 3, 4, 5 and 6 (open circle) are HotQCD simulations with  $2 + 1$  flavor at finite temperature [35]. They are reliably extrapolated to the continuum limit. Various thermodynamic quantities are deduced as functions of temperature at vanishing chemical potential. Their reliable continuum extrapolated results on the equation of state have been performed with stout-smearred staggered action [73]. At high temperature, this action effectively reduces taste symmetry violation effects, which remain large for  $\mathcal{O}(a^2)$  cutoff, where  $a$  is the lattice spacing [73]. The current continuum extrapolated results [35] are obtained with the HISQ action. They show an excellent agreement with the stout action [73]. The light-quark mass is fixed as a fraction of the strange-quark mass  $\hat{m}_l = \hat{m}_s/20$ . The results are obtained at lattice size  $N_\sigma^3 \cdot N_\tau$ , where  $N_\tau$  is temporal extent and  $N_\sigma$  is the spatial dimension.

It is apparent that the lattice QCD simulations at nonzero magnetic field  $eB \neq 0$  [36] give smaller quantities than that estimated in absence of the magnetic field [35]. In nonzero magnetic field, the system undergoes modifications due the presence of finite magnetization in the region of crossover region, where the magnetic field contribution to the suppression in the chiral condensate become large. To express the free energy as an integral over the longitudinal momentum, which is directed towards  $z$ -axis, i.e.,  $\mathbf{B} = B\hat{e}_z$ , and a summation over the *quantized* Landau levels, both should be performed numerically corresponding to Eqs. (12) and (15). Due to the occupation of the Landau levels, the thermal free-energy can be suppressed as the magnetic field grows [24].

In the present work, we aim to reproduce the recent lattice QCD calculations from PLSM. In doing this, we assume that the quark-hadron coupling constant  $g = 6.5$  and the Polyakov loop *deconfinement* temperatures,  $T = 187$  MeV in vanishing and finite magnetic field, respectively.

### 1. Trace anomaly

The normalized trace anomaly, which can be derived, directly, from the trace of the energy-momentum tensor,  $T_\nu^\mu = \epsilon - 3p$ , where  $\epsilon(p)$  being energy density (pressure), determines the degrees of freedom and helps in deducing further thermodynamic quantities such as energy density, pressure, and entropy density of the system of interest. In QCD, the trace anomaly can be related to the strong coupling constant,  $\propto T^4 \alpha_s^2$  [31]. This quantity vanishes in scale invariant theory such as massless, collisionfree gas of quarks and gluons. For a correlated gas (nonvanishing interactions), the QCD scale parameter remains finite. The QCD asymptotic freedom implies that the strength of the interaction weakens with the temperature [far above the critical temperature ( $T_c$ )]. At temperatures smaller than  $T_c$ , the trace anomaly increases with the temperature because more massive hadrons become relevant.

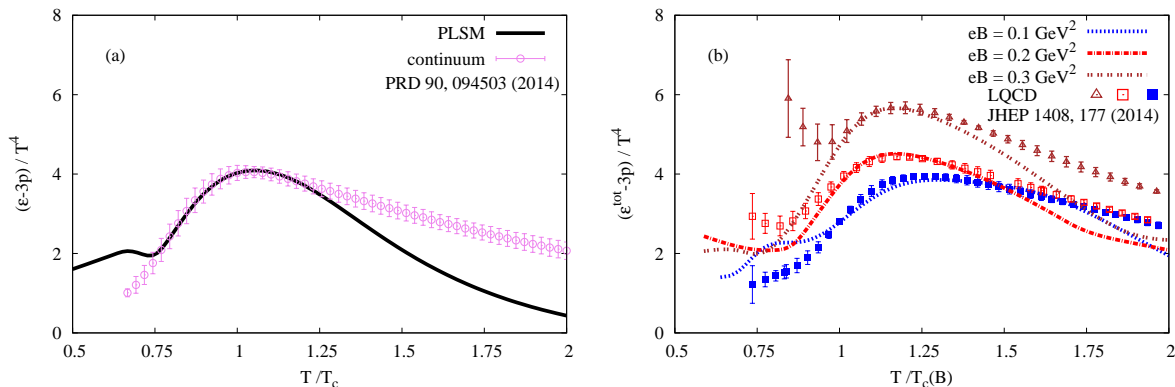


**Fig. 3:** (Color online) Left-hand panel (a): the normalized trace-anomaly,  $(\epsilon - 3p)/T^4$ , as a function of temperature compared with lattice QCD calculations extrapolated to the continuum limit are given as open circles [35]. Right-hand panel (b): the normalized trace anomaly at different values of magnetic fields  $eB = 0.1$  (dotted curve),  $eB = 0.2$  (dotted-dash curve) and  $eB = 0.3$  GeV<sup>2</sup> (double-dotted curve) compared with the recent lattice QCD (close square), (open square) and (open triangle), respectively [36].

In Fig. 3, the temperature dependence of the normalized trace-anomaly calculated from PLSM at vanishing [left-hand panel (a)] and nonzero magnetic field [right-hand panel (b)]. In left-hand panel (a), the trace anomaly

normalized to  $T^4$  in given in comparison with lattice QCD calculations extrapolated to continuum limit [35]. There is a well agreement with the lattice QCD simulations, especially in the hadronic phase. This is also obvious near the phase transition region. At higher temperatures, a repaid decrease occurs in the interaction measurement. It is faster than in the lattice QCD simulations.

In right-hand panel of Fig. 3 (b), the modified, normalized trace anomaly, Eq. (28), is depicted as a function of temperature. The thermodynamic modifications due to the presence of finite magnetization have been discussed in the previous section. Our PLSM calculations are also given at different values of magnetic field strengths,  $eB = 0.1$  (dotted curve),  $eB = 0.2$  (dotted-dash curve) and  $eB = 0.3 \text{ GeV}^2$  (double-dotted curve) and compared with recent lattice QCD [36] (close square), (open square) and (open triangle), respectively.

As discussed in the previous section, the thermodynamic quantities, which are derived from the free energy, are accordingly modified, especially due to the presence of finite magnetization. The latter measures the response of the system of interest to applying finite magnetic field. In finite magnetic field, the free energy from PLSM is calculated as an integral over the longitudinal momentum along the direction of magnetic field  $\mathbf{B} = B\hat{e}_z$  and a summation over the *quantized* Landau levels. Adding finite magnetization for the free energy affects various thermodynamic quantities. Furthermore, due to the occupation of the Landau levels, the thermal free energy suffers from an additional suppression with increasing magnetic field. Thus, the total energy-density likely differs from the quantity depicted in the left-hand panel (a).

In the hadron phase, the trace anomaly becomes very small at low temperature, but increases with the temperature. A peak appears at the critical temperature. A further increase in the temperature decreases the trace anomaly, i.e., derives the system strongly into the deconfined status. The trace anomaly signals breaking of the scale invariance in the system of interest. Its peak around  $T_c$  is conjectured to signal anomalous thermodynamic properties, for example, the bulk viscosity, which measures how easy or difficult for the system to relax back to equilibrium after going through scale transformation. This would mean that the peak of the trace anomaly refers to maximum bulk viscosity, that is likely when the breaking of scale invariance becomes maximum.

## 2. Speed of sound squared

Analogy to the hydrodynamical approaches, which have been applied on the relativistic heavy-ion collisions and led to the RHIC discovery of the new state of QCD matter [74], the speed of sound squared ( $c_s^2$ ) plays an essential role in estimating the equation of state  $p(\rho)$ . As discussed in Ref. [38], the definition of  $c_s^2$  as in Eq. (29) means that the energy fluctuations and other collective phenomena associated with the specific heat are not taken into account.

The speed of sound squared is related to the trace anomaly ( $\Delta = \epsilon - 3p$ ), where the conformal measure is given as

$$\mathcal{C} = \frac{\Delta}{\epsilon} = \frac{\epsilon - 3p}{\epsilon} \approx 1 - 3c_s^2, \quad (32)$$

which becomes maximum around the region of the phase transition, in which the speed of sound squared becomes small. At high temperatures, the speed of sound squared reaches the Stefan-Boltzmann (SB) limit of  $1/3$ . In this limit, the conformal measure obviously vanishes. In left-hand panel of Fig. 4 (a), the temperature dependence of the speed of sound squared calculated from the ratio  $s/c_v$  and  $p/\epsilon$  are compared with recent lattice QCD calculations with continuum extrapolation [35]. The right-hand panel (b) illustrates the ratio  $p/\epsilon$  as a function of temperature and compares the PLSM calculations with the recent lattice QCD in finite magnetic field [36].

Left-hand panel of Fig. 4 (a) shows PLSM results on  $p/\epsilon$  (dashed curve) and on  $s/c_v$  (solid curve) and compares them with lattice QCD calculations extrapolated to the continuum limits [35]. The lattice QCD results on both  $c_s^2$ , (open circles) and  $p/\epsilon$ (open tangles) are extrapolated to the continuum limits.

Both quantities  $p/\epsilon$  and  $s/c_v$  are apparently confirmed from in the continuum extrapolation of lattice QCD [35]. Above  $T_c$ , PLSM seems to overestimate  $s/c_v$ . At lower temperature, the opposite temperature-dependence is observed. It is apparent that  $c_s^2$  (solid curve) matches  $p/\epsilon$  (dashed curve). The PLSM and lattice QCD calculations confirm that there is a difference between  $c_s^2$ , (open circles)  $p/\epsilon$  (open tangles). The agreement is improved in the hadron phase but becomes poor in high temperature. In high-temperature region, PLSM overestimates the lattice calculations.

It is worthwhile to highlight that the temperature dependence of  $c_s^2$  seems to be sensitive to the normalization to  $T_c$ . The lattice calculations are given in dependence on  $T$ , which is normalized to  $T_c \sim 181 \pm 9 \text{ MeV}$ , while

the PLSM calculations are normalized to chiral restoration-temperature  $T_\chi \sim 240$  MeV. Also, it is obvious that the speed of sound squared  $c_s^2$  approaches the Stefan-Boltzmann limit, i.e.  $1/3$ , at very high temperatures. The peak, which appears near the critical temperature, is due to the fast rate of the change of energy density with increasing temperature.

Furthermore, the right-hand panel of Fig. 4 (b) presents PLSM calculations of  $p/\epsilon$  at  $eB = 0.1$  (dotted curve),  $eB = 0.2$  (dotted-dash curve) and  $eB = 0.3$  GeV<sup>2</sup> (double-dotted curve) and compared to recent lattice QCD [36] (close square), (open square) and (open triangle), respectively. A good agreement is obtained, especially at low temperature. It is obvious that the agreement can be improved with increasing the magnetic field strength. It is noteworthy highlighting that the agreement looks better than that at  $eB = 0$ .

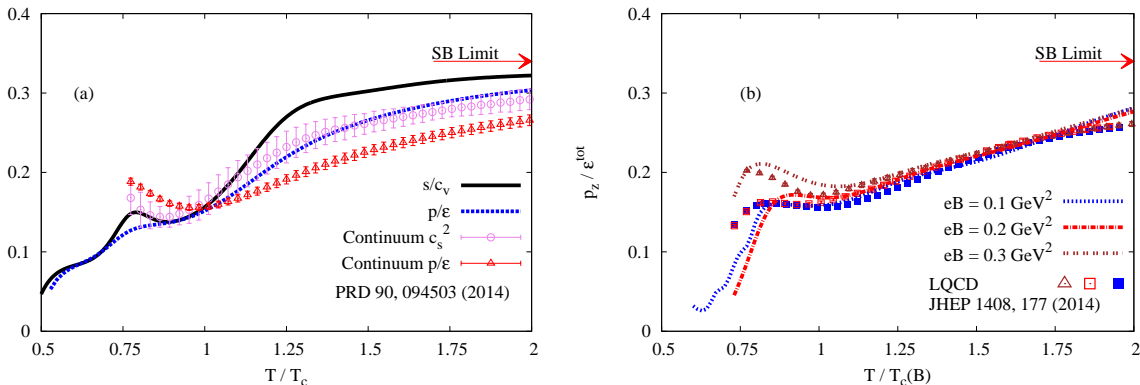


**Fig. 4:** (Color online) Left-hand panel (a): the speed of sound squared calculated as a function of temperature from  $s/c_v$  (solid curve) and  $p/\epsilon$  (dotted curve) compared with lattice QCD calculations extrapolated to the continuum limit are given as open circles [35]. Right-hand panel (b): in finite magnetic field, the ratio  $p/\epsilon$  at  $eB = 0.1$  (dotted curve),  $eB = 0.2$  (dotted-dash curve) and  $eB = 0.3$  GeV<sup>2</sup> (double-dotted curve) is compared with the recent lattice QCD (close square), (open square) and (open triangle), respectively [36].

### 3. Entropy

Eq. (22) expresses the explicit dependence of the free energy-density on the temperature, the chemical potential and the magnetic field strength. Per definition, in B-scheme, the background magnetic field directed along  $z$ -axis, the thermal pressure is isotropic. The entropy can be estimated from Eq. (24). Left-hand panel of Fig. 5 (a) shows the normalized entropy ( $s/T^3$ ) in a wide range of temperatures at vanishing chemical potential and vanishing magnetic field. The temperature dependence continues even above  $T_c$ , i.e.,  $s/T^3$  keeps its rise with increasing  $T/T_c$ . Then it becomes slightly higher than lattice results. The dependence on the magnetic field is presented in the right-hand panel (b). The temperature dependence of normalized entropy density ( $s/T^3$ ) [left-hand panel (a)] is calculated from PLSM at vanishing chemical potential and compared with recent lattice QCD simulations which are extrapolated to the continuum limit [35], as well as with the lattice QCD with p4 action and  $N_\tau = 8$  (open triangles) [67] and  $N_\tau = 10$  (solid circles) [67]. A reasonable agreement with the lattice QCD simulations is obvious and the phase transitions seems to take place, smoothly. The temperature dependence continues above  $T_c$ , i.e.,  $s/T^3$  keeps increasing with increasing  $T/T_c$  until it becomes slightly lower than lattice results.

### 4. Specific heat

In the previous section, we have characterized the temperature dependence of the entropy density in zero and finite magnetic field. Besides entropy density the specific heat ( $c_v$ ) can be used in charactering the equation of state, i.e., speed of sound squared. For a wide range of temperatures and at vanishing chemical potential, PLSM calculations on  $c_v$  are compared with recent lattice QCD [35] in the left-hand panel of Fig. 6 (a). The PLSM results indicate a reasonable agreement with the lattice QCD at low and high temperatures. The peak that appears at  $T_c$  can be interpreted from the definition of the specific heat;  $c_v = \partial\epsilon/\partial T$ . It is apparent that

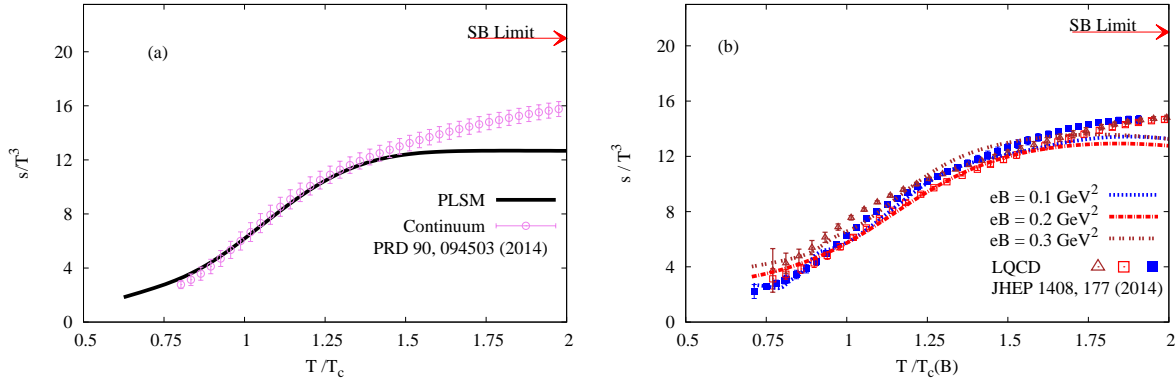


**Fig. 5:** (Color online) Left-hand panel (a): the normalized thermal entropy density  $s/T^3$  (solid curve) given as a function of temperature is compared with the lattice QCD calculations extrapolated to the continuum limit are given as open circles [35]. Right-hand panel (b) compares between the PLSM calculations at  $eB = 0.1$  (dotted curve),  $eB = 0.2$  (dotted-dash curve) and  $eB = 0.3 \text{ GeV}^2$  (double-dotted curve) and the recent lattice QCD (solid square), (open square) and (open triangle), respectively [36].

the peak might be due to the rapid change in the energy density around  $T_c$ . Furthermore, the appearance of the peak would be strongly related to the chemical potential. In a previous work, we have shown that the peak declines with increasing chemical potential [22]. The specific heat grows with increasing temperature. Apart from the PLSM peak that appears at the transition temperature, the specific heat approaches the corresponding SB-limit at high temperatures. The deviation SB limits might be due to the differences in the contributing gluon degrees of freedom. The overall agreement with the lattice QCD [35] is excellent.

The right-hand panel (b) presents normalized specific heat as derived from modified free-energy, Eq. (22), due to finite magnetization ( $\mathcal{M}$ ) as a function of temperature at vanishing chemical potential and different magnetic field strengths,  $eB = 0.0$  (solid curve),  $eB = 0.1$  (dotted curve) and  $eB = 0.3 \text{ GeV}^2$  (double-dotted curve). Unfortunately, no lattice QCD calculations exist to compare our PLSM results with. We notice that the deviation from SB-limit is relatively large.

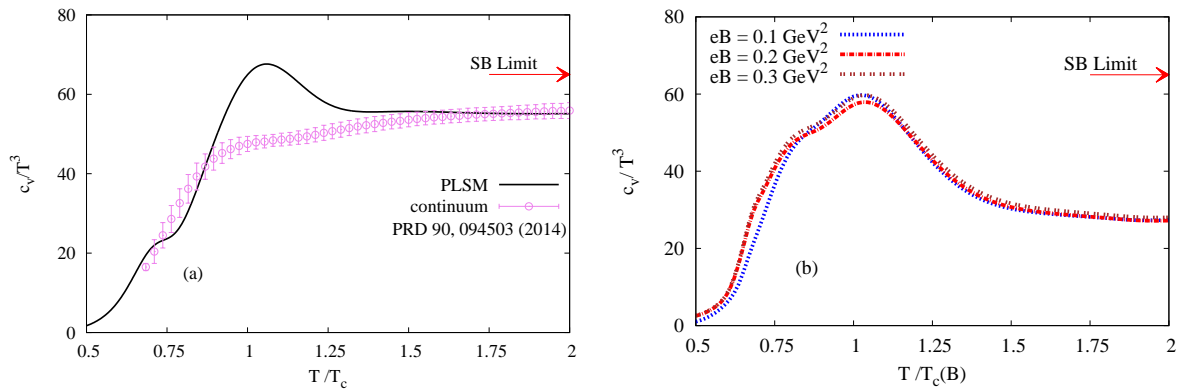


**Fig. 6:** (Color online) Left-hand panel shows the temperature dependence of the normalized specific heat  $c_v/T^3$  calculated from PLSM at vanishing chemical potential (solid curve) and compared with the continuum limits (open circles) [35]. Right-hand panel: the influence of the magnetic field strength on QCD matter is illustrated at  $eB = 0.0$  (solid curve),  $eB = 0.1$  (dotted curve) and  $eB = 0.3 \text{ GeV}^2$  (double-dotted curve).

## 5. Magnetization and magnetic catalysis

As introduced in section III B, the magnetization largely affects the thermodynamic properties of strongly interacting QCD matter. The magnetization refers to the response of the system of interest on the applied magnetic field, which is very likely in HIC. Because of the relativistic, off-center motion of the spectators in peripheral collisions (motion of electric charge generates magnetic field perpendicular to plane of both motion direction and electric field) and because of local imbalance in the momenta that are carried by the colliding nucleons in peripheral and even central collisions (such local imbalance leads to angular momentum and thus magnetic field) [75]. Such magnetic field can be very huge,  $\mathcal{O}(m_\pi^2)$ , i.e. very much larger than the detector magnet field.

The magnetization ( $\mathcal{M}$ ) can be derived from Eq. (25) in  $\text{GeV}^2$  natural units. The sign of magnetization signals an important magnetic property of the system of interest. In our case, the QCD matter is *para*- or *dia*-magnetic if  $\mathcal{M} > 0$  or  $\mathcal{M} < 0$ , respectively. Furthermore, from solid state physics, we borrow that

- in *dia*-magnetic QCD matter, the thermal QCD medium aligns oppositely to the direction of the magnetic field and produces an induced electric current, which spreads as small loops attempting to cancel the effects of the applied magnetic field, and
- in *para*-magnetic QCD matter, the thermal QCD medium aligns towards the direction of the magnetic field.

In middle panel of Fig. 7 (b), the magnetization  $\mathcal{M}$  is given as a function of temperatures at  $eB = 0.1$  (dotted),  $0.2$  (dashed),  $0.3$  (double-dotted) and  $0.4 \text{ GeV}^2$  (dash-dotted curve) at vanishing chemical potential. The results are compared with recent lattice QCD [36] at  $eB = 0.1$  (closed square),  $0.2$  (open circle),  $0.3$  (open triangle) and  $0.4 \text{ GeV}^2$  (astride). It is apparent that the sign of the magnetization is positive and  $\mathcal{M} > 0$  increases with the magnetic field. The positive sign of magnetization indicates that the paramagnetic contribution of QCD matter becomes dominant with increasing temperature. Within the temperature range characterizing the hadron phase (below  $T_c$ ), the PLSM curve seems to resemble the lattice data in an excellent way. At temperatures characterizing QGP (above  $T_c$ ), the PLSM curve becomes larger than the lattice data, especially at very high temperatures. In this range of temperatures, the hadrons are conjectured to deconfine into color, quark and gluon degrees of freedom. It seems that these degrees of freedom are not sufficient enough to achieve a good agreement at very high temperature. Furthermore, PLSM has a temperature-limited applicability depending on the temperature-applicability of its order parameters, section II. Only within this limit the capability of PLSM to characterize the magnetic properties of hot QCD matter is guaranteed.

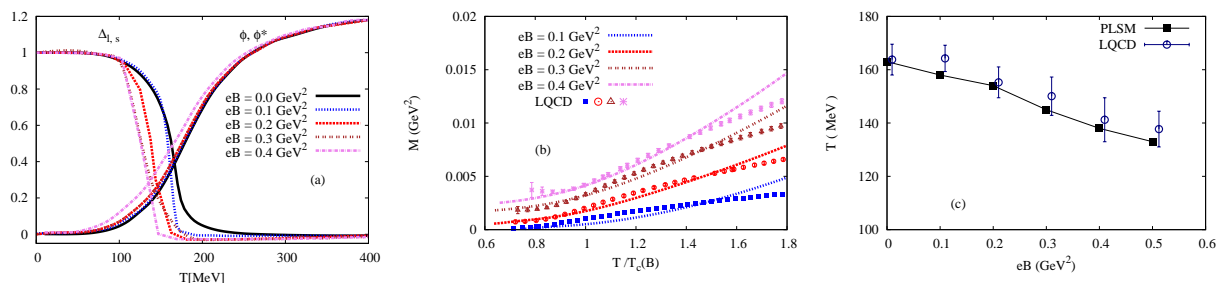


**Fig. 7:** (Color online) Left-hand panel (a): the subtracted chiral-condensates and the deconfinement phase transitions at different values of magnetic field  $eB = 0.0$  (solid curves),  $eB = 0.1$  (dotted curves),  $eB = 0.2$  (dashed curves),  $eB = 0.3$  (double-dotted curves) and  $eB = 0.4 \text{ GeV}^2$  (dotted-dash curves). Middle panel (b): the magnetization in  $\text{GeV}^2$ -units is determined as a function of temperature from PLSM and compared with recent lattice QCD calculations in the presence of magnetic fields [36]. Right-hand panel (c) depicts the dependence of the critical temperature on the magnetic field strengths (both quantities are given in physical units) as determined from PLSM (solid symbols) is compared with lattice QCD calculations (open symbols) [36].

In addition to the modifications in the thermodynamic quantities due to the finite magnetic field, which are mainly determined by the magnetization ( $\mathcal{M}$ ), it intends now to characterize the magnetic catalysis. As in quantum electrodynamic (QED), the magnetic catalysis describes how the magnetic field dynamically generates masses. Furthermore, the Meissner effect describes how the magnetic field changes the order of the phase transition in type-I superconductor. These two phenomena are borrowed to study the possible influence of finite magnetic field on the QCD phase-space structure [7, 8] and/or the response of hadronic and partonic matter to nonzero magnetic field in thermal and dense medium [24].

The inclusion of finite magnetic field in the QCD-effective models is achieved through modification in the phase space, energy-momentum dispersion relations and Landau levels occupations. Various works such as [76–78, 80–82] have been devoted to characterize the magnetic catalysis. Accordingly, the critical temperatures increase as the magnetic field increases. On the other hand, other works have concluded a decrease in the critical temperature as the magnetic field increases [80–82]. In Ref. [77], it was argued that the increase in  $T_c(B)$  with the magnetic field is possible unless some parameters are fine-tuned and the coupling constant is assumed to vary with the magnetic field, i.e.,  $g(B)$ . Furthermore, it was remarked that  $T_0(B)$  does not enable PLSM to reproduce  $T_c(B)$  as deduced from lattice QCD calculations, especially in magnetic field strengths  $eB \leq 1 \text{ GeV}^2$ . In the present work, it intends to reproduce recent lattice QCD calculations from PLSM calculations. In doing this, we assume that the quark-hadron coupling constant  $g = 6.6$  and the Polyakov loop deconfinement temperatures  $T_0 = 270$  and  $187 \text{ MeV}$  in vanishing finite magnetic field, respectively.

The main difference between this present work and literature is the outcome from the free energy at finite volume, Eq. (15). We find that the free energy at  $eB = 0$  is utilized in Eq. (15). While at finite values of  $eB$ ,  $\delta_{0,eB}$  becomes active. The delta function vanishes at all finite values of  $eB$  and vice versa. Accordingly, we dis- or in-clude the last term of Eq. (15). We conclude that temperature dependence of the thermodynamic quantities at finite magnetic fields are smaller than those at zero magnetic field. This means that the results are shifted to lower, e.g. smaller  $T_c$  as well, with increasing magnetic field.

In this regards, there are two different mechanisms. The first one is that the magnetic field improves the phase-transition due to its contributions to the Landau quantizations or levels. The second mechanism assumes that, the magnetic field contributes to the suppression in the chiral condensates relevant to the restoration of the chiral symmetry breaking. This suppression is known as inverse magnetic catalysis and manifests a decrease in the chiral critical temperature with increasing magnetic field.

The left-hand panel of Fig. 7 (a) illustrates the subtracted chiral-condensates and the deconfinement phase transition at different values of magnetic field  $eB = 0.0$  (solid curves),  $eB = 0.1$  (dotted curves),  $eB = 0.2$  (dashed curves),  $eB = 0.3$  (double-dotted curves) and  $eB = 0.4 \text{ GeV}^2$  (dotted-dash curves). The increase in the magnetic field strength suppresses the chiral condensate relevant to the restoration of the chiral symmetry breaking. Again, the earliness of the chiral-condensate expiration (suppression) relative to the temperature points to chiral magnetic catalysis, where the critical temperature ( $T_c$ ) decreases with increasing the magnetic field. Accordingly, we can extract the variation of the critical temperature with raising the magnetic field in right-hand panel (c) of Fig. 7.

The right-hand panel of Fig. 7 (c) shows the variation of the critical temperature with increasing magnetic field at vanishing chemical potential. The PLSM critical temperature is to be estimated from the intersection point (in temperature axis) between the subtracted chiral condensate  $\Delta_{l,s}$  and the deconfinement phase transition. It is apparent that the critical temperature decreases with the magnetic field. Furthermore, the PLSM calculations indicate a good agreement with recent lattice QCD simulation [36].

#### IV. CONCLUSIONS

In the present work, we have combined SU(3) linear-sigma model with the Polyakov-loop corrections in order to address the deconfinement phase-transition and characterize the chiral quark-meson structure. The PLSM calculations indicate that the chiral condensates ( $\sigma_l$  and  $\sigma_s$ ) and deconfinement order parameters or Polyakov loops ( $\phi$  and  $\phi^*$ ) are relatively sensitive to the magnetic field strength. The other order parameters of this model such as  $M_b$  and subtracted condensate  $\Delta_{l,s}$  have a much better agreement with the recent lattice QCD simulations. In case of vanishing magnetic field, we observe a fair matching with the lattice QCD calculations, especially for the restoration of broken chiral symmetry. This phase transition is not prompt but rather a *slow* crossover. Increasing the magnetic field strength tends to suppress the chiral phase-transition and decrease the quasi-chiral temperatures. Concretely, we found that the chiral temperatures for light-quark condensate  $T_\chi^{(l)}$  decreases faster than the chiral temperatures for strange-quark condensate  $T_\chi^{(s)}$ .

The PLSM in the presence of finite magnetic field assumes some restrictions to be added to the quarks due to the existence of free charges in the plasma phase. The Yukawa coupling of quarks seems to play an essential role in achieving an excellent agreement with recent lattice QCD. Furthermore, the QCD system undergoes modifications due to the presence of finite magnetization. The free energy is given as an integral over the longitudinal momentum, which is directed towards  $z$ -axis, and then we apply Landau theory (Landau quantization), which quantizes of the cyclotron orbits of charged particles in magnetic field. Accordingly, we find that the value of the chiral condensates is suppressed with increasing the magnetic field.

Furthermore, in mean field approximation, we have constructed the partition function and then estimated various thermodynamic quantities, such as trace anomaly (interaction measure), speed of sound squared, entropy density, specific heat and the magnetization. Their dependence on temperature highlights the effects of magnetic field on therm in both hadron and parton phases. We have compared our calculations with recent lattice simulations at vanishing chemical potential and finite magnetic field [35]. We conclude that our calculations with a scalar coupling parameter simulate well the lattice QCD calculation in nonzero magnetic field [36].

At low temperature, a good agreement between PLSM and lattice QCD simulations is found. In this temperature limit, the meson fluctuations in the mean field approximation are dominated. Similarly, at high temperature, the gluon dynamics is not fully accomplished by the Polyakov-loop corrections. This explains the discrepancy with the lattice QCD calculations. As concluded from the hadron resonance gas model [38], the quantities  $\partial p/\partial\epsilon$  and  $s/c_v$  should not be necessarily identical. The difference between partial and complete differentiation might partly explain this at least from the mathematical point-of-view. The physical point-of-view proposes that  $\partial p/\partial\epsilon$  and  $s/c_v$  do not take into consideration the same types of fluctuations. In an intensive study, Tawfik *et al.* specified that the main differences between  $\partial p/\partial\epsilon$  and  $s/c_v$  are the energy fluctuations [38]. In deriving specific heat, several types of energy density susceptibilities, fluctuations and multiplicities appear [38, 83]. A list of such fluctuations are listed in Appendix A of Ref [38]. An evidence supporting this interpretation has been reported, recently [84]. The most solid support for this study is offered by the phenomenological lattice QCD calculations [39]. Accordingly,  $\partial p/\partial\epsilon$  and  $s/c_v$  differ from each other, especially below and above  $T_c$ . At  $T < T_c$ ,  $c_s^2 = \partial p/\partial\epsilon$  is larger than  $c_s^2 = s/c_v$ , while at  $T > T_c$ ,  $c_s^2 = s/c_v$  becomes larger than  $c_s^2 = \partial p/\partial\epsilon$ . At  $T > 2 - 3T_c$ , both expressions get very close to each other until they approach the asymptotic value, i.e., 1/3. The lattice simulations do not propose any reason why  $\partial p/\partial\epsilon$  and  $s/c_v$  should not be identical. We conclude that increasing the magnetic field strength increases the thermodynamic quantities, especially in the hadron phase. At high temperatures, the PLSM thermodynamics is apparently limited below the Stefan-Boltzmann limits. Furthermore, we find that the quark-hadron phase boundary is shifted to lower values of temperatures with increasing magnetic field strength.

The sign of magnetization signals para- or dia-magnetic property of QCD matter. The excellent agreement between PLSM and recent lattice calculations means that our PLSM gives a well-suited description for the degrees of freedom in both hadron and parton phases. The magnetic field seems to enhance the occurrence of chiral phase-transition due to its contributions to the Landau quantizations. The magnetic field also contributes to the suppression in the chiral condensates relevant to the restoration of the chiral symmetry-breaking. This suppression is known as the inverse magnetic catalysis and seems to manifest a decrease in the chiral critical temperature with increase magnetic field.

It is noteworthy highlighting that the results estimated from PLSM in vanishing and finite magnetic field can be trusted within the limits of the numerical calculations of the PLSM order parameters,  $\sigma_l$ ,  $\sigma_s$ ,  $\phi$  and  $\phi^*$  in thermal and dense QCD medium. In this regard, one has to recall that PLSM has a temperature-limited applicability depending on the temperature-applicability of its chiral and deconfinement order-parameters. Only within this limit the conclusions drawn about the equation of state, the magnetic properties of the QCD matter and the chiral phase-structure, etc. can be relatively certain.

- 
- [1] Y. Nambu and G. Jona-Lasinio, "Dynamical Model of Elementary Particles Based on an Analogy with Superconductivity. I", Phys. Rev. **122**, 345 (1961).
  - [2] Y. Nambu and G. Jona-Lasinio, "Dynamical Model of Elementary Particles Based on an Analogy with Superconductivity. II", Phys. Rev. **124**, 246 (1961).
  - [3] M. Gell-Mann and M. Levy, "The axial vector current in beta decay", Il Nuovo Cimento **16**, 705 (1960).
  - [4] D. E. Kharzeev, L. D. McLerran, and H. J. Warringa, Nucl. Phys. A **803**, 227 (2008).
  - [5] V. Skokov, A. Illarionov, and V. Toneev, Int. J. Mod. Phys. A **24**, 5925 (2009).
  - [6] A. Bzdak and V. Skokov, Phys. Lett. B **710**, 174 (2012);  
W. Deng and X. Huang, Phys. Rev. C **85**, 044907 (2012).
  - [7] E. S. Fraga and A. J. Mizher, Nucl. Phys. A **831**, 91 (2009).
  - [8] E. S. Fraga and A. J. Mizher, Phys. Rev. D **78**, 025016 (2008).
  - [9] A. V. Zayakin, JHEP **0807**, 116 (2008); G. Lifschytz and M. Lippert, Phys. Rev. D **80**, 066005 (2009);  
G. Lifschytz and M. Lippert, Phys. Rev. D **80**, 066007 (2009);  
H. U. Yee, JHEP **0911**, 085 (2009);  
S. I. Cui, Y. h. Gao, Y. Seo, S. j. Sin and W. s. Xu, Phys. Rev. D **81**, 066001 (2010);  
E. DHoker and P. Kraus, JHEP **1003**, 095 (2010).

- [10] K. Fukushima, Phys. Rev. D **77**, 114028 (2008);  
K. Fukushima, D. E. Kharzeev, and H. J. Warringa, Phys. Rev. D **78**, 074033 (2008).
- [11] S. P. Klevansky and R. H. Lemmer, Phys. Rev. D **39**, 3478 (1989).
- [12] V. P. Gusynin, V. A. Miransky, and I. A. Shovkovy, Phys. Lett. B **349**, 477 (1995);  
V. P. Gusynin, V. A. Miransky, and I. A. Shovkovy, Nucl. Phys. B **462**, 249 (1996).
- [13] G. W. Semenoff, I. A. Shovkovy, and L. C. R. Wijewardhana, Phys. Rev. D **60**, 105024 (1999).
- [14] A. Goyal and M. Dahiya, Phys. Rev. D **62**, 025022 (2000).
- [15] B. Hiller, A. A. Osipov, A. H. Blin, and J. da Providencia, SIGMA **4**, 024 (2008).
- [16] E. Rojas, A. Ayala, A. Bashir, and A. Raya, Phys. Rev. D **77**, 093004 (2008).
- [17] S. P. Klevansky, Rev. Mod. Phys. **64**, 649 (1992).
- [18] K. G. Klimenko, "Magnetic catalysis and oscillating effects in Nambu-Jona-Lasinio model at nonzero chemical potential", arXiv:hep-ph/9809218.
- [19] A. Y. Babansky, E. V. Gorbar, and G. V. Shchepanyuk, Phys. Lett. B **419**, 272 (1998).
- [20] D.P. Menezes, M.B. Pinto, S.S. Avancini, A.P. Martinez, and C. Providencia, Phys. Rev. C **79**, 035807 (2009).
- [21] K. Fukushima, M. Ruggieri, and R. Gatto, Phys. Rev. D **81**, 114031 (2010).
- [22] A. Tawfik and N. Magdy, Phys. Rev. C **91**, 015206 (2015).
- [23] A. Tawfik and N. Magdy, Phys. Rev. C **90**, 015204 (2014).
- [24] A. Tawfik and A. Diab, and M. T. Hussein, "Chiral Magnetic Effects from Extended  $SU(3)$  Linear-Sigma Model", in press.
- [25] T. D. Cohen, D. A. McGady, and E. S. Werbos, Phys. Rev. C **76**, 055201 (2007).
- [26] N. O. Agasian and I. A. Shushpanov, Phys. Lett. B **472**, 143 (2000).
- [27] A. Tawfik, N. Magdy, and A. Diab, Phys. Rev. C **89**, 055210 (2014).
- [28] A. Tawfik and A. Diab, *Polyakov  $SU(3)$  extended linear  $\sigma$ -model: Sixteen mesonic states in chiral phase-structure*, Phys. Rev. C **91**, 015204 (2015).
- [29] A. Tawfik and N. Magdy, *Thermodynamics and higher order moments in  $SU(3)$  linear -model with gluonic quasi-particles*, J. Phys. G **42**, 015004 (2015) .
- [30] M. Ruggieri, M. Tachibana, and V. Greco, JHEP **1307**, 165 (2013).
- [31] A. Tawfik, "Constant Trace Anomaly as a Universal Condition for the Chemical Freeze-Out", Phys. Rev. C **88**, 035203 (2013).
- [32] R. Gatto and M. Ruggieri, Lect. Notes Phys. **871**, 87 (2013).
- [33] D. E. Kharzeev, K. Landsteiner, A. Schmitt, and H. U. Yee, Lect. Notes Phys. **871**, 1 (2013).
- [34] Jens O. Andersen, William R. Naylor, and Anders Tranberg, "Phase diagram of QCD in a magnetic field: A review", 1411.7176 [hep-ph].
- [35] A. Bazavov *et al.*, Phys. Rev. D **90**, 094503 (2014).
- [36] G. S. Bali, F. Bruckmann, G. Endrodi, S.D. Katz, and A. Schafer, JHEP **1408**, 177 (2014).
- [37] P. Castorina, J. Cleymans, D. E. Miller, and H. Satz, Eur. Phys. J. C **66**, 207-213 (2010).
- [38] A. Tawfik and H. Magdy, Int. J. Mod. Phys. A **29**, 1450152 (2014).
- [39] S. Borsanyi, G. Endrodi, Z. Fodor, S.D. Katz, S. Krieg, C. Ratti, and K.K. Szabo, JHEP **1208**, 053 (2012).
- [40] I. A. Shovkovy, Lect. Notes Phys. **871**, 13 (2013).
- [41] F. Preis, A. Rebhan, and A. Schmitt, "Inverse magnetic catalysis in dense holographic matter", JHEP **1103**, 033 (2011).
- [42] M. D. Elia, S. Mukherjee, and F. Sanfilippo, Phys. Rev. D **82**, 051501 (2010).
- [43] A. Haber, F. Preis, and A. Schmitt, Phys. Rev. D **90**, 125036 (2014).
- [44] M. Ferreira, P. Costa, C. Providencia, O. Lourenco, and T. Frederico, "Inverse Magnetic Catalysis in hot quark matter within  $(P)NJL$  models", 1504.01313 [hep-ph].
- [45] N. N. Ajitanand, R. A. Lacey, A. Taranenko, and J. M. Alexander, Phys. Rev. C **83**, 011901 (2011).
- [46] B. I. Abelev, *et al.*, Phys. Rev. Lett. **103**, 251601 (2009).
- [47] B. I. Abelev, *et al.*, Phys. Rev. C **81**, 054908 (2010).
- [48] S. A. Voloshin, Indian J. Phys. **85**, 1103 (2011).
- [49] L. Adamczyk, *et al.*, Phys. Rev. Lett. **113**, 052302 (2014).
- [50] I. Selyuzhenkov, *et al.*, Prog. Theor. Phys. Suppl. **193**, 153 (2012).
- [51] O. Scavenius, A. Mocsy, I. N. Mishustin, and D. H. Rischke, Phys. Rev. C **64**, 045202 (2001).
- [52] S. Weinberg, "Gravitation and Cosmology", (Wiley, New York, 1972).
- [53] B.-J. Schaefer and J. Wambach, Phys. Rev. D **75**, 085015 (2007).
- [54] L. M. Haas, R. Stiele, J. Braun, J. M. Pawlowski, and J. Schaffner-Bielich, Phys. Rev. D **87**, 076004 (2013).
- [55] C. Ratti, *et al.*, Phys. Rev. D **73**, 014019 (2005).
- [56] S. Rossner, C. Ratti, and W. Weise, Phys. Rev. D **75**, 034007 (2007).
- [57] A. M. Polyakov, "Thermal Properties Of Gauge Fields And Quark Liberation", Phys. Lett. B **72**, 477 (1978).
- [58] L. Susskind, "Lattice Models Of Quark Confinement At High Temperature", Phys. Rev. D **20**, 2610 (1979).
- [59] E. Nakano, B.-J. Schaefer, B. Stokic, B. Friman, and K. Redlich, Phys. Lett. B **682**, 401 (2010).
- [60] B.-J. Schaefer, J. M. Pawlowski, and J. Wambach, Phys. Rev. D **76**, 074023 (2007).
- [61] J. I. Kapusta and C. Gale, "Finite-temperature field theory: Principles and applications", (Cambridge University

- Press, Cambridge, 2006).
- [62] J. K. Boomsma and D. Boer, Phys. Rev. D **81**, 074005 (2010).
  - [63] V. Skokov, B. Friman, E. Nakano, K. Redlich, and B.-J. Schaefer, Phys. Rev. D **82**, 034029 (2010).
  - [64] B. J. Schaefer and M. Wagner, Phys. Rev. D **79**, 014018 (2009).
  - [65] M. Cheng *et al.*, Phys. Rev. D **77**, 014511 (2008).
  - [66] A. Bazavov (HotQCD Collaboration) " *Chiral transition temperature and aspects of deconfinement in 2+1 flavor QCD with the HISQ/tree action*" **PoS LATTICE2011**, 182 (2011).
  - [67] A. Bazavov *et al.*, Phys. Rev. D **80**, 014504 (2009).
  - [68] M. Cheng *et al.*, Phys. Rev. D **81**, 054504 (2010).
  - [69] K. Orginos and D. Toussaint, Phys. Rev. D **59**, 014501 (1999);  
G.P. Lepage, Phys. Rev. D **59**, 074502 (1999);  
K. Orginos, D. Toussaint, and R. L. Sugar [MILC Collaboration], Phys. Rev. D **60**, 054503 (1999).
  - [70] U. M. Heller, F. Karsch, and B. Sturmfels, Phys. Rev. D **60**, 114502 (1999).
  - [71] A. Peikert, B. Beinlich, A. Bicker, F. Karsch, and E. Laermann, Nucl. Phys. Proc. Suppl. **63**, 895 (1998).
  - [72] L. Landau, E. Lifshitz, and L. Pitaevskii, " *Electrodynamics of continuous media. Course of theoretical physics*", (Butterworth-Heinemann, 1995).
  - [73] S. Borsanyi, G. Endrodi, Z. Fodor, A. Jakovac, S. D. Katz, *et al.*, JHEP **1011**, 077 (2010);  
S. Borsanyi, Z. Fodor, C. Hoelbling, S. D. Katz, S. Krieg, *et al.*, Phys. Lett. B **370**, 99 (2014).
  - [74] Miklos Gyulassy and Larry McLerran, " *New forms of QCD matter discovered at RHIC*", Nucl. Phys. A **750**, 30 (2005).
  - [75] A. Tawfik, " *QCD Phase-transition and chemical freezeout in nonzero magnetic field at NICA*", an invited contribution to EPJA Topical Issue "NICA White Paper"
  - [76] M. Ferreira, P. Costa, D. P. Menezes, C. Providencia, and N. Scoccola, Phys. Rev. D **89**, 016002 (2014), Addendum: Phys. Rev. D **89**, 019902 (2014).
  - [77] E.S. Fraga, B.W. Mintz, and J. Schaffner-Bielich, Phys. Lett. B **731**, 154 (2014).
  - [78] G. Cao, L. He, and P. Zhuang. Phys. Rev. D **90**, 056005 (2014).
  - [79] S. Mao, " *Magnetic Catalysis in Nambu–Jona-Lasinio Model beyond Mean Field*", arXiv:1602.06503 [hep-ph].
  - [80] M. Ferreira, P. Costa, O. Lourenco, and T. Frederico, Phys. Rev. D **89**, 116011 (2014).
  - [81] M. Ferreira, P. Costa, and C. Providencia, Phys. Rev. D **90**, 016012 (2014).
  - [82] R.L.S. Farias, V.S. Timoteo, S.S. Avancini, M.B. Pinto, and G. Krein, " *Thermo-magnetic effects in quark matter: Nambu–Jona-Lasinio model constrained by lattice QCD* ", arXiv:1603.03847 [hep-ph].
  - [83] George D. J. Phillies, " *Elementary lectures in statistical mechanics*", (Springer, New York, 2000).
  - [84] A. Tawfik, Adv. High Energy Phys. **2013**, 574871 (2013).
  - [85] E. Nakano, B.-J. Schaefer, B. Stokic, B. Friman, and K. Redlich, Phys. Lett. B **682**, 401 (2010).